ARTICLES

N-myristoyltransferase inhibitors as new leads to treat sleeping sickness

Julie A. Frearson[1], Stephen Brand[1], Stuart P. McElroy[1], Laura A. T. Cleghorn[1], Ondrej Smid[1], Laste Stojanovski[1], Helen P. Price[4], M. Lucia S. Guther[1], Leah S. Torrie[1], David A. Robinson[1], Irene Hallyburton[1], Chidochangu P. Mpamhanga[1], James A. Brannigan[3], Anthony J. Wilkinson[3], Michael Hodgkinson[4], Raymond Hui[5], Wei Qiu[5], Olawale G. Raimi[2], Daan M. F. van Aalten[2], Ruth Brenk[1], Ian H. Gilbert[1], Kevin D. Read[1], Alan H. Fairlamb[1], Michael A. J. Ferguson[1], Deborah F. Smith[4] & Paul G. Wyatt[1]

African sleeping sickness or human African trypanosomiasis, caused by *Trypanosoma brucei* spp., is responsible for ~30,000 deaths each year. Available treatments for this disease are poor, with unacceptable efficacy and safety profiles, particularly in the late stage of the disease when the parasite has infected the central nervous system. Here we report the validation of a molecular target and the discovery of associated lead compounds with the potential to address this lack of suitable treatments. Inhibition of this target—*T. brucei N*-myristoyltransferase—leads to rapid killing of trypanosomes both *in vitro* and *in vivo* and cures trypanosomiasis in mice. These high-affinity inhibitors bind into the peptide substrate pocket of the enzyme and inhibit protein *N*-myristoylation in trypanosomes. The compounds identified have promising pharmaceutical properties and represent an opportunity to develop oral drugs to treat this devastating disease. Our studies validate *T. brucei N*-myristoyltransferase as a promising therapeutic target for human African trypanosomiasis.

Protein *N*-myristoylation is a ubiquitous eukaryotic co- and post-translational modification and is required for the membrane targeting and biological activity of many important proteins[1,2]. The *N*-myristoylation reaction—the transfer of $C_{14:0}$ myristic acid from myristoyl-coenzyme A (CoA) to the amino group of amino-terminal glycine residues within specific sequence contexts[3]—is catalysed by the enzyme myristoyl-CoA-protein *N*-myristoyltransferase (NMT; International Union of Biochemistry and Molecular Biology accession EC 2.3.1.97)[4]. In *T. brucei*, NMT activity is encoded by a single gene, which has been shown to be essential for parasite growth using RNA interference[5]. The effects of NMT knockdown on *T. brucei* are probably complex as more than 60 proteins are predicted to be *N*-myristoylated in this organism[6]. Experimentally validated targets for NMT include ADP ribosylation factors (ARF)[7], ADP ribosylation-like factors (ARL)[8], a calpain-type protease (CAP5.5, systematic gene name Tb927.4.3950)[9] and, in the related *Leishmania major* and *T. cruzi* parasites, hydrophilic acylated surface proteins[10] and flagellar calcium-binding protein[11], respectively. The predicted pleiotropic effects of NMT inhibition on trypanosome physiology make it an attractive target for therapeutic intervention. NMT has also been considered as an anticancer[12], antifungal[13] and antiviral[14] target. Fungal NMT orthologues have been shown to be druggable, although broad-spectrum activity has not been achieved. Nevertheless, because there is good evidence from these programmes that selectivity over human NMT is possible, NMT has been proposed as a target for the treatment of human African trypanosomiasis and other parasitic diseases[15,16]. There are two human isozymes sharing 77% identity (HsNMT1 and HsNMT2)[17] of which HsNMT2 is the closest human homologue to *T. brucei* NMT (TbNMT), with overall 55% identity and 69% similarity. On the basis of 31 residues that are within 5 Å of DDD85646 in the active site, this rises to 83% identity and 90% similarity.

Pyrazole sulphonamide inhibitors of TbNMT

So far, no drug-like, potent inhibitors of TbNMT have been reported[18]. Screening of a 62,000 diversity-based compound library[19] against TbNMT identified a number of 'lead-like' hits, including a chemically tractable series with moderate potency (2 μM) based on a pyrazole sulphonamide scaffold (DDD64558). Optimization of the screening hit, involving the design and synthesis of over 200 compounds, identified highly potent inhibitors of TbNMT with single-digit nanomolar half-maximum inhibitory concentration (IC_{50}) values and levels of selectivity over human NMT enzymes in the 1- to >100-fold range (Fig. 1a). The relative lack of activity of the piperidine analogue (DDD85635) of DDD85602 indicated that the terminal basic nitrogen of DDD85602 was crucial for activity. The series was optimized by rigidifying the flexible linker to the amine moiety of DDD85602 and by adding the chlorines observed to give an increase in activity in the unelaborated template (DDD73234). TbNMT inhibitors so obtained (for example, DDD85646) inhibited the proliferation of bloodstream form *T. brucei* in culture with the best compounds yielding half-maximum effective concentration (EC_{50}) values between 0.8 and 3 nM and clear windows of selectivity (>200-fold) with respect to proliferation of a prototypical mammalian cell type (MRC5). We attribute the increased selectivity at the cellular level to differences in cell biology between host and parasite, although differential cellular pharmacokinetic behaviour has not been definitively ruled out. Critically, a tight correlation ($r^2 = 0.875$) was observed between IC_{50} and EC_{50} values for TbNMT and *T. brucei* proliferation, respectively, over a 10,000-fold potency range (Fig. 1b); this indicates that inhibition of TbNMT was driving the observed antiparasitic effect of these compounds. The poorer correlation for the most potent compounds (Fig. 1b, lower left) is probably due to the limit of the enzyme assay to provide accurate IC_{50} determinations

[1]Drug Discovery Unit, Division of Biological Chemistry and Drug Discovery, [2]Division of Molecular Microbiology, College of Life Sciences, University of Dundee, Dundee DD1 5EH, UK. [3]Structural Biology Laboratory, Department of Chemistry, [4]Centre for Immunology and Infection, Department of Biology and Hull York Medical School, University of York, Heslington, York YO10 5YW, UK. [5]Structural Genomics Consortium, University of Toronto, MaRS South Tower, 7th Floor, 101 College Street, Toronto, Ontario M5G 1L7, Canada.

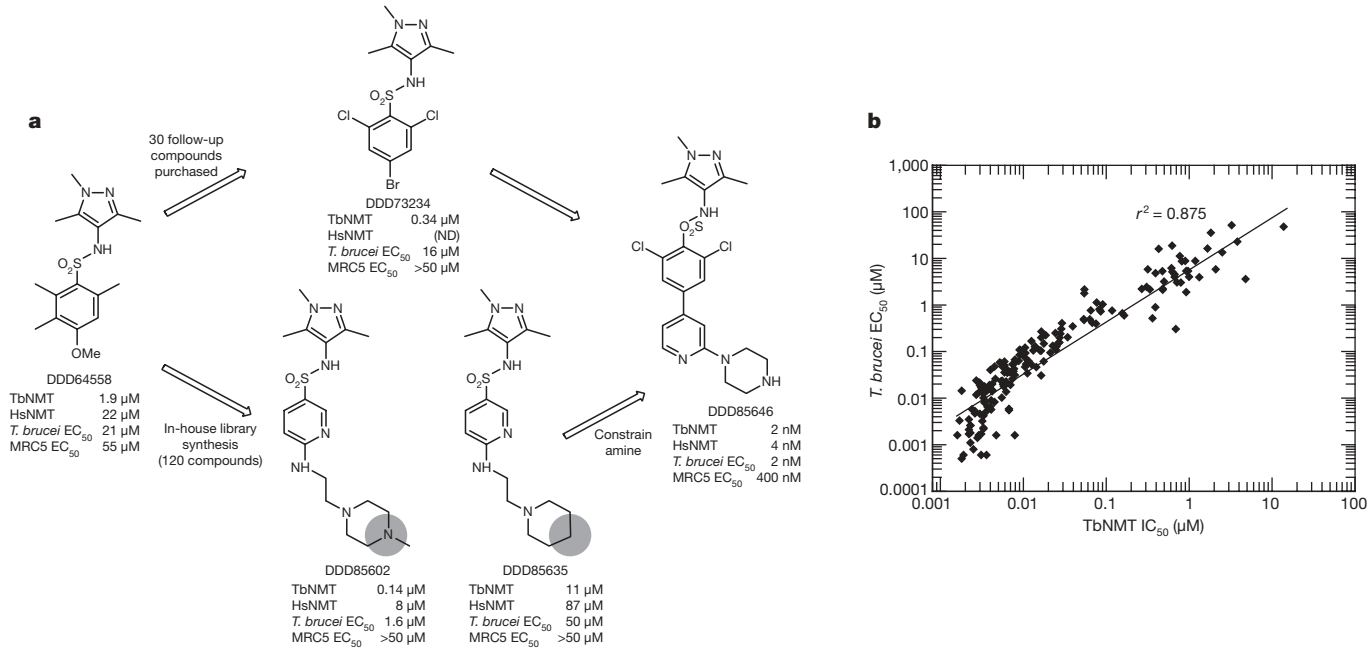

Figure 1 | Identification of NMT lead series inhibitors. a, Chemical evolution of DDD85646 from the initial high-throughput screening hit DDD64588. Combining the structure–activity relationships from the two strategies led to the development of the potent compound DDD85646. Potencies were determined for all compounds synthesized against recombinant TbNMT and HsNMT, as well as against bloodstream form *T. brucei* and MRC5 proliferation *in vitro*. ND, not determined. **b**, Correlation between the inhibition of recombinant TbNMT and bloodstream form *T. brucei* proliferation for 175 members of the pyrazole sulphonamide series. Data shown are replicates of between 2 and 22 independent potency determinations using 10-point curves. Robustness of TbNMT and trypanosome proliferation assays are exemplified through routinely reported parameters of Z' (0.703 ± 0.050, $n = 169$ and 0.695 ± 0.095, $n > 1{,}000$ for TbNMT and trypanosome assays, respectively) and reproducible potencies of standards (DDD73498 (TbNMT assay) $pIC_{50} = 6.52 \pm 0.14$, $n = 276$ and pentamidine (trypanosome assay) $pEC_{50} = 8.37 \pm 0.41$, $n = 497$), where p is the negative logarithm of the IC_{50} and EC_{50} values. r^2 is the square of the linear regression correlation coefficient.

for such highly active, tight-binding inhibitors (see Supplementary Fig. 1). As a result of its impressive potency in inhibiting both TbNMT and *T. brucei* proliferation *in vitro*, together with its promising physicochemical properties, DDD85646 was assessed for efficacy in animal models of trypanosomiasis.

TbNMT inhibitor cures acute trypanosomiasis *in vivo*

DDD85646 is moderately bioavailable (approximately 20%) and demonstrates good exposure after oral dosing at 10 and 50 mg kg^{-1} to female NMRI mice, with the free drug level above the effective concentration calculated to achieve 99% inhibition of parasite growth (EC_{99}) for *T. brucei brucei* (*T. b. brucei*) proliferation for over 6 and 10 h, respectively (Fig. 2a). Furthermore, this compound cured all animals in the *T. b. brucei* acute mouse model of human African trypanosomiasis at a minimal oral dose of 12.5 mg kg^{-1} (twice a day for 4 days) (Fig. 2b). Cure of all animals was also obtained with shorter oral dosing schedules: 100 mg kg^{-1} twice a day for 1 day and 25 mg kg^{-1} twice a day for 2 days. Notably, DDD85646 also cured all animals at 50 mg kg^{-1} (twice a day for 2 days) in the more refractory but clinically relevant *T. b. rhodesiense* model of human African trypanosomiasis (see Supplementary Fig. 2). This reduced sensitivity *in vivo* is not due to reduced sensitivity to the compound *in vitro* (*T. b. rhodesiense*, EC_{50} 0.6 nM), but may be a result of the known precedent for this species to occupy privileged sites *in vivo*. Notably, the efficacy observed for DDD85646 was comparable to the responses observed for the clinically used drugs pentamidine and melarsoprol in the *T. b. brucei* model (minimal full cure doses were 1 mg kg^{-1} and 0.5 mg kg^{-1} (intraperitoneal), respectively). Furthermore, despite the minimal window of *in vitro* enzyme selectivity between TbNMT and mammalian (human) NMT (Fig. 1a and see later), this compound was well tolerated at efficacious doses.

TbNMT inhibitors are trypanocidal

Addition of DDD85646 resulted in rapid killing of trypanosomes both *in vivo* and *in vitro* (Fig. 3a, b). Parasite counts dropped to below

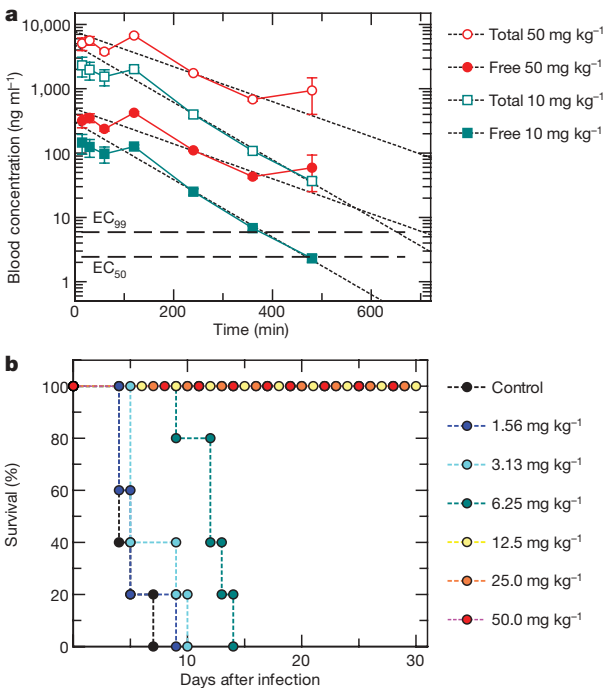

Figure 2 | TbNMT inhibitor cures acute trypanosomiasis *in vivo*. a, Mean total and free blood concentration time profiles after single oral administration of DDD85646 at 10 and 50 mg kg^{-1} free-base to female NMRI mice ($n = 3$ per dose group). EC_{99} is calculated from the average EC_{50} of 2.46 ± 1.8 nM and Hill slope of 4.84 ± 0.6 ($n = 5$). Solid lines are total plasma concentrations and dashed lines are the predicted free plasma concentrations (fraction unbound in plasma = 0.063). Data are mean ± s.d. **b**, Kaplan–Meier survival plot for female NMRI mice ($n = 5$ per dose group) after infection with *T. b. brucei* s427 (BS 221) (inoculum 1×10^4 parasites). Oral treatment with DDD85646 started 3 days after infection at the indicated doses (all twice a day for 4 days).

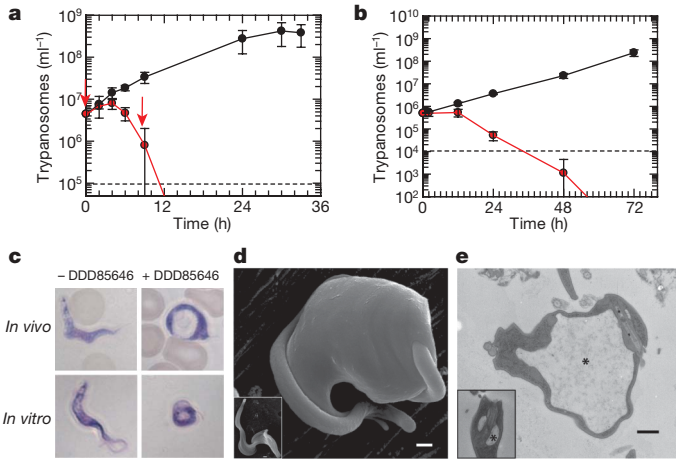

Figure 3 | TbNMT inhibitors have rapid trypanocidal effects *in vitro* and *in vivo*. **a**, Parasitaemia in mice ($n = 3$ per group) with (red) or without (black) DDD85646 treatment (50 mg kg^{-1}, oral, twice a day); for method see Fig. 2b. Arrows represent dose administration times. Data are mean ± s.d. **b**, *T. b. brucei* proliferation in culture determined by counting motile parasites in the presence (red) or absence (black) of 50 nM DDD85646. Data are mean ± s.d. for 3 determinations. **c**, Blood smears of infected mice and culture samples were stained by Giemsa and observed by light microscopy. Treated cells showed typical BigEye phenotype. **d**, Scanning electron micrograph of *T. b. brucei* treated with 10 nM DDD85646 for 24 h. Inset shows an untreated control cell. **e**, Transmission electron micrograph of sagittal section of flagellar pocket of *T. b. brucei* treated with 5 nM DDD85646 for 72 h. Inset shows a section of flagellar pocket of an untreated control cell. Asterisks mark flagellar pockets. Dashed lines, cell detection limits. Scale bars, 500 nm.

detectable levels within 12 h of dosing mice at 50 mg kg^{-1} twice a day. Addition of DDD85646 (50 nM) to bloodstream form *T. brucei* cultures *in vitro* also resulted in rapid killing with numbers of motile cells reduced to below detectable levels between 24 and 48 h. The apparent differences in the kinetics of death between the *in vivo* and *in vitro* systems are probably a combination of the harsher *in vivo* environment for drug-damaged trypanosomes and the fact that compound exposure reached higher concentrations *in vivo* (up to ~1 μM), compared with 50 nM *in vitro*.

The trypanocidal mechanism of compound action was confirmed by subjecting *T. brucei* treated *in vitro* with 50 nM DDD85646 to live/dead fluorescence-activated cell sorting (FACS) analysis, which showed >95% cell death within 24 h of treatment (see Supplementary Fig. 3). Furthermore, wash-out experiments showed that death was irreversible after 48 h of exposure to 50 nM compound (data not shown). Microscopic examination of the trypanosomes treated with DDD85646 *in vivo* and *in vitro* showed the same abnormal morphology, that is, the development of a large vesicular structure (Fig. 3c). A scanning electron micrograph of a treated trypanosome clearly shows the rounded and swollen features of this phenotype compared to control (Fig. 3d). Notably, rapid cell killing with a similar morphological phenotype has been previously observed after treatment with myristate analogues, such as 10-(propoxy)decanoic acid[20]. This morphology closely resembles the 'BigEye' phenotype observed in bloodstream form *T. brucei* when endocytosis is disrupted by the knockdown of clathrin heavy chain, TbRAB5[21,22] or TbARF1[7], leading to expansion of the flagellar pocket. Parasites with enlarged flagellar pockets are clearly visible in the DDD85646-treated trypanosome population (Fig. 3e). Additional studies are required to understand fully the cellular effects of NMT inhibition.

Inhibitor acts 'on target'

Incubation of bloodstream form *T. brucei* with [^{3}H]myristic acid results in the biosynthetic radiolabelling of myristoylated substrates, particularly the highly abundant variant surface glycoprotein (VSG)[23]. Using this method, but including a detergent lysis step that activates an endogenous phospholipase C (PLC) to release the [^{3}H]myristate label from the glycosylphosphatidylinositol (GPI) anchor of VSG[24], a number of putative *N*-[^{3}H]myristoylated proteins were visualized by SDS–polyacrylamide gel electrophoresis (PAGE) and fluorography (Fig. 4a, lane 2). The labelling of most of these proteins was eliminated by prior treatment with DDD85646 (Fig. 4a, lane 1). To confirm that most of the proteins labelled with [^{3}H]myristic acid were indeed *N*-myristoylated, a duplicate gel was treated with 0.2 M NaOH in methanol before fluorography to remove base-labile hydroxy- or thioester linked [^{3}H]myristate (Fig. 4a, lanes 3 and 4). Three faint DDD85646-insensitive bands were removed (Fig. 4a, compare lanes 1 and 2 with lanes 3 and 4); these probably include traces of residual GPI-anchored VSG at 55 kilodalton (kDa)[24] and thioester-myristoylated GPI-PLC at 42 kDa[25]. To assess whether DDD85646 specifically inhibited *N*-[^{3}H]myristoylation, the same cells were labelled in parallel with [^{35}S]methionine. Pre-treatment of parasites with DD85646 had no effect on [^{35}S]methionine incorporation into proteins, showing that the compound has no effect on general protein synthesis (Fig. 4a, lanes 5 and 6).

Further evidence that DDD85646 was acting on target in the trypanosome was obtained by overexpressing TbNMT (fivefold) in a tetracycline-inducible manner; this resulted in an eightfold reduction in DDD85646 potency against these cells (Fig. 4b).

Another independent approach was taken using one of the few known substrates of TbNMT in *T. brucei*, TbARF1. This protein has a central role in endocytosis and Golgi–lysosome trafficking, where tetracycline-induced expression of a constitutively active GTP-locked mutant (Q71L) causes rapid cell death in bloodstream form *T. brucei* in an *N*-myristoylation-dependent manner[7]. Short-term treatment (5 h) with 10 nM DDD85646 rescued these TbARF1(Q71L)-expressing cells from death (Fig. 4c), presumably by preventing *N*-myristoylation of newly produced TbARF1(Q71L) protein. Although the Q71L mutant protein could not be detected by western blotting, as previously reported [7], the inducible expression of the related, but myristoylation-blocked, G2A/Q71L mutant in the presence of DDD85646 does show that its effect on cell survival was not due to interference with tetracycline induction of these mutants.

Taken together, these data provide strong evidence that DDD85646 acts to inhibit TbNMT in bloodstream form trypanosomes and that this is directly linked to inhibition of proliferation. These data also provide a potential link between inhibition of TbNMT and disruption of the function of the TbNMT substrate TbARF1, known to operate in protein trafficking and endocytic processes.

Inhibitor binds in TbNMT peptide pocket

The target product profile for a new drug to combat human African trypanosomiasis, as defined by the Drugs for Neglected Diseases initiative, requires compounds that are safe and efficacious against both the stage 1 disease, when parasites are present in the blood, lymph and interstitial fluids, and the stage 2 disease, when parasites are also present in the central nervous system (CNS). The DDD85646 compound does not yet meet these criteria and will have to be optimized for selectivity over human NMT and for diffusion into the CNS, while retaining excellent potency against TbNMT and bloodstream form *T. brucei* cells. To achieve these objectives, a detailed understanding of the interaction between DDD85646 and TbNMT is required. Characterization of the mode of inhibition of the early hits revealed competition with the peptide substrate as a probable mode of inhibition for the series. Thus, a shift in IC_{50} from 1 to 4.3 μM for an early hit was seen when the peptide substrate concentration in the assay was increased from 0.5 to 16 μM (Fig. 5a). Surface plasmon resonance (SPR) studies confirmed a 1:1 binding stoichiometry of DDD85646 with TbNMT (Fig. 5b) and showed that the binding affinity of the compound was increased in the presence of myristoyl-CoA from 33 nM to 1 nM (data not shown). Accurate determination of binding

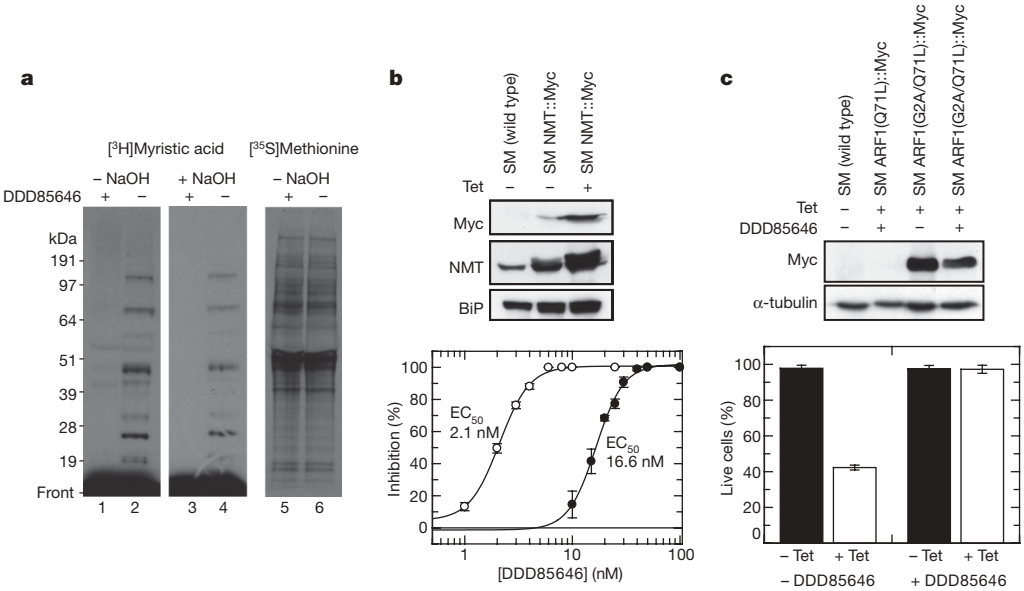

Figure 4 | Pyrazole sulphonamide series acts 'on target' in the trypanosome. **a**, Fluorographs of SDS–PAGE gels loaded with lysates of bloodstream form *T. b. brucei* cells labelled with either [^{3}H]myristic acid (lanes 1–4) or [^{35}S]methionine (lanes 5 and 6) after pre-incubation with (+) or without (−) 0.5 μM DDD85646 for 6 h. Gels were incubated with or without 0.2 M NaOH in MeOH, as indicated, before fluorography. **b**, Wild-type ('single marker', SM) parasites and *T. b. brucei* overexpressing Myc-tagged NMT were incubated with 0–100 nM DDD85646 for 64 h; motile cells were counted using a haemocytometer. Filled circles, *T. brucei* overexpressing NMT ($n = 3$); open circles, wild-type cells ($n = 3$). Levels of Myc-tagged NMT expression were confirmed by western blotting. **c**, *T. b. brucei* expressing ARF1(Q71L) (GTP-locked form of ARF1) under tetracycline control were treated with 10 nM DDD85646 for 6 h. Cells were then subjected to live/dead FACS analysis. Data shown represent mean ± s.d. from two independent experiments. Levels of Myc-tagged ARF1 mutant expression were analysed by western blotting. Tet, tetracycline. BiP, binding protein, an endoplasmic reticulum chaperone.

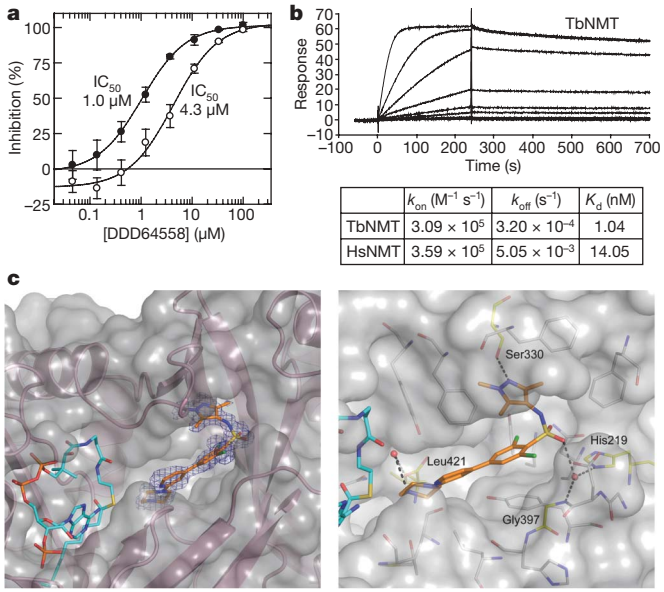

	k_{on} (M^{-1} s^{-1})	k_{off} (s^{-1})	K_d (nM)
TbNMT	3.09×10^5	3.20×10^{-4}	1.04
HsNMT	3.59×10^5	5.05×10^{-3}	14.05

Figure 5 | Characterization of pyrazole sulphonamide interactions with NMT. **a**, DDD64558 potency against TbNMT (IC_{50}) determined in the presence of 0.5 μM (filled circles) and 16 μM (open circles) CAP5.5 peptide substrate. Each data point represents mean ± s.d. ($n = 4$). **b**, Kinetics of binding of DDD85646 to TbNMT and HsNMT1 determined by SPR. k_{on} or k_a is the second-order rate constant for association and k_{off} or k_d is the first-order rate constant for dissociation, where the dissociation constant $K_d = k_{off}/k_{on}$. **c**, X-ray crystal structure of DDD85646 bound to LmNMT. The left panel shows the LmNMT binding site with protein backbone (pink ribbon), solvent accessible surface (grey), DDD85646 (stick representation, carbon atoms gold, nitrogen blue, chlorine green, oxygen red and sulphur yellow), myristoyl CoA (carbon atoms cyan) and an omit map ($F_o - F_c$, 3.0 sigma) around DDD85646 (blue). The right panel shows a stick representation of DDD85646 and residues forming the active site (carbon atoms grey). Key residues are highlighted (carbon atoms yellow) as are water molecules (red spheres) and hydrogen bonds (dashed lines).

affinity using SPR also showed a potential small window of selectivity between TbNMT and human NMT with binding constants of 1 and 14 nM, respectively. Owing to tight binding of this compound (see Supplementary Fig. 1), this selectivity was less clear in the biochemical assay, which recorded 2 and 4 nM (IC_{50}), respectively. Furthermore, this emerging selectivity is clearly driven by differing off-rates, and optimization around this parameter will not only be important in improving selectivity, but also in sustaining a high residency time of binding to TbNMT. The structure of TbNMT has yet to be solved. However, using *L. major* NMT (LmNMT) as a model system, the binding of DDD85646 in the peptide substrate binding site has been confirmed by X-ray crystallography (Fig. 5c, for stereo view see Supplementary Fig. 4). LmNMT has 74% overall sequence identity with TbNMT and 94% identity within the peptide-binding site (see Supplementary Fig. 5). The binding mode shows the piperazine interacting with the carboxy-terminal carboxylate of NMT by means of a tightly coordinated water molecule as opposed to a direct hydrogen bond. The sulphonamide makes water-bridged interactions with the highly conserved residue His 219 and with the backbone NH group of Gly 397. The geometry of the sulphonamide creates a significant bend in the structure, allowing the pyrazole to fit into a lipophilic pocket where it acts as a hydrogen-bond acceptor from Ser 330. The binding mode is of particular interest because all but the latter interactions are through water-mediated hydrogen bonds; a mode not readily predicted using computational techniques. Overlaying the structure of *Saccharomyces cerevisiae* NMT in complex with substrate peptide (Protein Data Bank accession 1IID)[26] with the LmNMT complex shows that DDD85646 occupies the peptide binding site with the basic piperazine moiety mimicking the N terminus of the substrate (see Supplementary Fig. 6).

Conclusions

We have presented evidence that our model TbNMT inhibitor, DDD85646, kills bloodstream form *T. brucei* by acting on TbNMT *in situ*. There are probably several downstream consequences of TbNMT inhibition in the parasite, as the enzyme has over 60 putative

substrates[6], and this no doubt explains the speed of killing and the marked morphological changes observed on treatment with this compound. The emergence of the BigEye phenotype, and the possible link to TbARF1 activity, suggests that disturbance of endocytosis is one mechanism by which TbNMT inhibitors act in bloodstream form *T. brucei*. Interestingly, knockdown of TbNMT levels in bloodstream form *T. brucei* by RNA interference to 16% of wild-type levels, although fatal *in vitro* and *in vivo*, does not lead to the BigEye phenotype but rather to the accumulation of vesicles close to the flagellar pocket[27].

It is notable that, despite the small window of selectivity between human NMT and TbNMT, DDD85646 shows promising selectivity at the cellular level. One might speculate that *T. brucei* cells are hypersensitive to NMT inhibition because of unique or unusual aspects of their biochemistry and/or cell biology. In this context, the extremely high endocytic rate of bloodstream form *T. brucei* (some 9 times faster than fibroblasts and 2.6 times faster than macrophages), combined with the entire endocytic/exocytic process occurring in the flagellar pocket, is noteworthy[28]. The parasite's requirement for this high endocytic rate relates to its need to remove antibody from the cell surface and to recycle the protective VSG coat[29].

Finally, we may conclude that TbNMT is one of the few *T. brucei* proteins that has been comprehensively validated as a drug target for human African trypanosomiasis. The TbNMT inhibitors described meet many requirements for a greatly needed new therapeutic agent for human African trypanosomiasis. Further optimization of this series towards improved CNS penetration and selectivity is currently underway. In the meantime, DDD85646 will serve as an excellent chemical tool for investigation of the biology of protein *N*-myristoylation across a range of organisms.

METHODS SUMMARY

Enzyme activity assays were performed in scintillation proximity format[18], with minor modifications. Proliferation assays were performed using resazurin as an indicator of metabolic activity[30]. TbNMT was immobilized onto NTA sensor chips using standard immobilization protocols and kinetics of binding of compound analysed on Biacore T-100. Details of all standard methods including compound exposure studies and efficacy studies, metabolic labelling, microscopy and crystallography can be found in Methods. Chemical synthesis details can be found in Supplementary Materials.

Full Methods and any associated references are available in the online version of the paper at www.nature.com/nature.

Received 30 September 2009; accepted 10 February 2010.

1. Farazi, T. A., Waksman, G. & Gordon, J. I. The biology and enzymology of protein *N*-myristoylation. *J. Biol. Chem.* **276,** 39501–39504 (2001).
2. Resh, M. D. Trafficking and signaling by fatty-acylated and prenylated proteins. *Nature Chem. Biol.* **2,** 584–590 (2006).
3. Maurer-Stroh, S., Eisenhaber, B. & Eisenhaber, F. N-terminal *N*-myristoylation of proteins: prediction of substrate proteins from amino acid sequence. *J. Mol. Biol.* **317,** 541–557 (2002).
4. Bhatnagar, R. S., Futterer, K., Waksman, G. & Gordon, J. I. The structure of myristoyl-CoA: protein *N*-myristoyltransferase. *Biochim. Biophys. Acta* **1441,** 162–172 (1999).
5. Price, H. P. *et al.* Myristoyl-CoA: protein *N*-myristoyltransferase, an essential enzyme and potential drug target in kinetoplastid parasites. *J. Biol. Chem.* **278,** 7206–7214 (2003).
6. Mills, E., Price, H. P., Johner, A., Emerson, J. E. & Smith, D. F. Kinetoplastid PPEF phosphatases: dual acylated proteins expressed in the endomembrane system of *Leishmania*. *Mol. Biochem. Parasitol.* **152,** 22–34 (2007).
7. Price, H. P., Stark, M. & Smith, D. F. *Trypanosoma brucei* ARF1 plays a central role in endocytosis and Golgi-lysosome trafficking. *Mol. Biol. Cell* **18,** 864–873 (2007).
8. Price, H. P., Panethymitaki, C., Goulding, D. & Smith, D. F. Functional analysis of TbARL1, an *N*-myristoylated Golgi protein essential for viability in bloodstream trypanosomes. *J. Cell Sci.* **118,** 831–841 (2005).
9. Hertz-Fowler, C., Ersfeld, K. & Gull, K. CAP5.5, a life-cycle-regulated, cytoskeleton-associated protein is a member of a novel family of calpain-related proteins in *Trypanosoma brucei*. *Mol. Biochem. Parasitol.* **116,** 25–34 (2001).
10. Denny, P. W., Gokool, S., Russell, D. G., Field, M. C. & Smith, D. F. Acylation-dependent protein export in *Leishmania*. *J. Biol. Chem.* **275,** 11017–11025 (2000).
11. Wingard, J. N. *et al.* Structural insights into membrane targeting by the flagellar calcium-binding protein (FCaBP), a myristoylated and palmitoylated calcium sensor in *Trypanosoma cruzi*. *J. Biol. Chem.* **283,** 23388–23396 (2008).
12. Selvakumar, P. *et al.* Potential role of *N*-myristoyltransferase in cancer. *Prog. Lipid Res.* **46,** 1–36 (2007).
13. Georgopapadakou, N. H. Antifungals targeted to protein modification: focus on protein *N*-myristoyltransferase. *Expert Opin. Investig. Drugs* **11,** 1117–1125 (2002).
14. Hill, B. T. & Skowronski, J. Human *N*-myristoyltransferases form stable complexes with lentiviral Nef and other viral and cellular substrate proteins. *J. Virol.* **79,** 1133–1141 (2005).
15. Bowyer, P. W. *et al.* *N*-myristoyltransferase: a prospective drug target for protozoan parasites. *ChemMedChem* **3,** 402–408 (2008).
16. Sheng, C. *et al.* Homology modeling and molecular dynamics simulation of *N*-myristoyltransferase from protozoan parasites: active site characterization and insights into rational inhibitor design. *J. Comput. Aided Mol. Des.* **23,** 375–389 (2009).
17. Giang, D. G. & Cravatt, B. F. A second mammalian *N*-myristoyltransferase. *J. Biol. Chem.* **273,** 6595–6598 (1998).
18. Panethymitaki, C. *et al.* Characterization and selective inhibition of myristoyl-CoA: protein *N*-myristoyltransferase from *Trypanosoma brucei* and *Leishmania major*. *Biochem. J.* **396,** 277–285 (2006).
19. Brenk, R. *et al.* Lessons learnt from assembling screening libraries for drug discovery for neglected diseases. *ChemMedChem* **3,** 435–444 (2008).
20. Doering, T. L. *et al.* An analog of myristic acid with selective toxicity for African trypanosomes. *Science* **252,** 1851–1854 (1991).
21. Allen, C. L., Goulding, D. & Field, M. C. Clathrin-mediated endocytosis is essential in *Trypanosoma brucei*. *EMBO J.* **22,** 4991–5002 (2003).
22. Hall, B., Allen, C. L., Goulding, D. & Field, M. C. Both of the Rab5 subfamily small GTPases of *Trypanosoma brucei* are essential and required for endocytosis. *Mol. Biochem. Parasitol.* **138,** 67–77 (2004).
23. Ferguson, M. A. J. & Cross, G. A. M. Myristylation of the membrane form of a *Trypanosoma brucei* variant surface glycoprotein. *J. Biol. Chem.* **259,** 3011–3015 (1984).
24. Ferguson, M. A. J., Low, M. G. & Cross, G. A. M. Glycosyl-*sn*-1,2-dimyristylphosphatidylinositol is covalently linked to *Trypanosoma brucei* variant surface glycoprotein. *J. Biol. Chem.* **260,** 4547–4555 (1985).
25. Armah, D. A. & Mensa-Wilmot, K. *S*-myristoylation of a glycosylphosphatidylinositol-specific phospholipase C in *Trypanosoma brucei*. *J. Biol. Chem.* **274,** 5931–5938 (1999).
26. Farazi, T. A., Waksman, G. & Gordon, J. I. Structures of *Saccharomyces cerevisiae* *N*-myristoyltransferase with bound myristoylCoA and peptide provide insights about substrate recognition and catalysis. *Biochemistry* **40,** 6335–6343 (2001).
27. Price, H. P., Guther, M. L., Ferguson, M. A. & Smith, D. F. Myristoyl-CoA:protein *N*-myristoyltransferase depletion in trypanosomes causes avirulence and endocytic defects. *Mol. Biochem. Parasitol.* **169,** 55–58 (2010).
28. Overath, P. & Engstler, M. Endocytosis, membrane recycling and sorting of GPI-anchored proteins: *Trypanosoma brucei* as a model system. *Mol. Microbiol.* **53,** 735–744 (2004).
29. Engstler, M. *et al.* Hydrodynamic flow-mediated protein sorting on the cell surface of trypanosomes. *Cell* **131,** 505–515 (2007).
30. Patterson, S. *et al.* Synthesis and evaluation of 1-(1-(benzo[*b*]thiophen-2-yl)cyclohexyl)piperidine (BTCP) analogues as inhibitors of trypanothione reductase. *ChemMedChem* **4,** 1341–1353 (2009).

Supplementary Information is linked to the online version of the paper at www.nature.com/nature.

Acknowledgements This work was supported by grants from the Wellcome Trust (WT077705, WT083481, WT077503 and WT085622), Scottish Funding Council (HR04013) and by the Translational Biology Theme of SULSA. We thank the European Regional Development Fund and the Wolfson Foundation for grants that provided relevant infrastructure for this work. The Structural Genomics Consortium is a registered charity (number 1097737) that receives funds from the Canadian Institutes for Health Research, the Canadian Foundation for Innovation and Genome Canada through the Ontario Genomics Institute, GlaxoSmithKline, Karolinska Institutet, the Knut and Alice Wallenberg Foundation, the Ontario Innovation Trust, the Ontario Ministry for Research and Innovation, Merck, the Novartis Research Foundation, the Swedish Agency for Innovation Systems, the Swedish Foundation for Strategic Research and the Wellcome Trust. We would like to thank all members of the Drug Discovery Unit for their technical assistance in this study, particularly B. Rao, I. Collie and D. James.

Author Contributions The project management team responsible for experimental design and coordination of research activities comprised S.B., R.B., A.H.F., M.A.J.F., J.A.F., I.H.G., K.D.R., D.M.F.vA., P.G.W. and D.F.S. J.A.B., M.H. and A.J.W. optimized expression and produced the active TbNMT used for screening in the Drug Discovery Unit. Biological studies were carried out by S.P.M., O.S., L.S.T., M.L.S.G., I.H. and H.P.P.; chemical syntheses by L.A.T.C. and S.B.; structural biology and modelling by D.A.R., O.G.R., C.P.M., R.H. and W.Q.; and pharmacological studies by L.S.

Author Information Atomic coordinates and structure factors for the crystal structures have been deposited with the Protein Data Bank under accession codes 3H5Z and 2WSA for LmNMT with bound myristoyl CoA and with bound DDD85646, respectively. Reprints and permissions information is available at www.nature.com/reprints. The authors declare competing financial interests: details accompany the full-text HTML version of the paper at www.nature.com/nature. Correspondence and requests for materials should be addressed to P.G.W. (p.g.wyatt@dundee.ac.uk).

METHODS

Determination of exposure in rat after acute oral dosing. Female NMRI mice (25–35 g; Harlan Laboratories; $n = 3$ per dose group) were administered DDD85646 at 10 and 50 mg kg^{-1} orally. The dose solutions were prepared on the day of dosing and the vehicle was 5% dimethylsulphoxide (DMSO) in deionized water, or 5% DMSO and 40% PEG400 in deionized water, respectively. Blood samples (10 µl) were collected from the tail vein of each animal into micronic tubes (Micronic BV) containing deionized water (20 µl) at 0.25, 0.5, 1, 2, 4, 6 and 8 h post-dose and stored at −80 °C to await analysis.

Sample extraction of blood was performed by a method based on protein precipitation using acetonitrile and a structural analogue of the analyte of interest as internal standard. Blood extracts were analysed by UPLC/MS/MS using a Quattro Premier XE mass spectrometer (Waters). Calibration curves were constructed in blood to cover at least three orders of magnitude (that is, 1–1,000 ng ml^{-1}).

Efficacy studies. DDD85646 was tested *in vivo* against *T. b. brucei* using a modification of the approach described[31]. In brief, female NMRI mice (25–35 g; Harlan Laboratories; 3–5 per group) were injected intraperitoneally with 1×10^4 bloodstream forms of *T. b. brucei* strain s427 (also known as BS 221 or MITaT 1.2). These bloodstream forms come from a stock of cryopreserved stabilates containing 10% glycerol. The stabilate was suspended in phosphate-saline-glucose to obtain a trypanosome concentration of 5×10^4 ml^{-1}. Each mouse was injected with 0.2 ml. DDD85646 was administered orally from day 3 to day 6 of the experiment and parasitaemia levels monitored up to day 30. Animals with parasitaemia $>10^8$ ml^{-1} were humanely killed as previous studies had shown that animals do not survive a further 24 h[32]. The day on which mice were killed was recorded.

NMT enzyme assay. NMT assays[18,33] were carried out at room temperature (22–23 °C) in 384-well white optiplates (Perkin Elmer). Each assay was performed in a 40 µl reaction volume containing 30 mM Tris buffer, pH 7.4, 0.5 mM EDTA, 0.5 mM EGTA, 1.25 mM dithiothreitol (DTT), 0.1% (v/v) Triton X-100, 0.125 µM [^{3}H]myristoyl-coA (8 Curie (Ci) mmol^{-1}), 0.5 µM biotinylated CAP5.5, 5 nM NMT and various concentrations of the test compound. The IC_{50} values for HsNMT1 and HsNMT2 were essentially identical against 80 compounds tested and, for logistical reasons, only HsNMT1 was used in later studies.

Test compound (0.4 µl in DMSO) was transferred to all assay plates using a Cartesian Hummingbird (Genomics Solution) before 20 µl of enzyme was added to assay plates. The reaction was initiated with 20 µl of a substrate mix and stopped after 15 min (HsNMT1 or HsNMT2) or 50 min (TbNMT) with 40 µl of a stop solution containing 0.2 M phosphoric acid, pH 4.0 and 1.5 M $MgCl_2$ and 1 mg ml^{-1} PVT SPA beads (GE Healthcare). All reaction mix additions were carried out using a Thermo Scientific WellMate (Matrix). Plates were sealed and read on a TopCount NXT Microplate Scintillation and Luminescence Counter (Perkin Elmer).

ActivityBase from IDBS was used for data processing and analysis. All IC_{50} curve fitting was undertaken using XLFit version 4.2 from IDBS. A four-parameter logistic dose response curve was used using XLFit 4.2 Model 205. All test compound curves had floating top and bottom and pre-fit was used for all four parameters.

Compound efficacy and trypanocidal activity in cultured *T. brucei* parasites. Bloodstream *T. b. brucei* s427 were cultured at 37 °C in modified HMI9 medium (56 µM 1-thioglycerol was substituted for 200 µM 2-mercaptoethanol) and quantified using a haemocytometer. For the live/dead assay, cells were analysed using a two-colour cell viability assay (Invitrogen) as described previously[7]. Routine screening of test compounds against parasites was performed in 96-well plates using a modification[30] of the cell viability assay previously described[34]. Cell culture plates were stamped with 1 µl of an appropriate concentration of test compound in DMSO followed by the addition of 200 µl trypanosome culture (10^4 cells ml^{-1}) to each well, except for one column which received media only. MRC5 cells were cultured in DMEM, seeded at 2,000 cells per well and allowed to adhere overnight. One-microlitre of test compound (10 point dilutions from 50 µM to 2 nM) was added to each well at the start of the assay. Culture plates of *T. brucei* and MRC5 cells were incubated at 37 °C in an atmosphere of 5% CO_2 for 69 h, before the addition of 20 µl resazurin (final concentration, 50 µM). After a further 4 h incubation, fluorescence was measured (excitation 528 nm; emission 590 nm) using a BioTek flx800 plate reader.

SPR analysis. The interaction between NMT and DDD85646 was assessed using a Biacore T100 instrument. Histidine-tagged TbNMT and HsNMT1 were immobilized onto an NTA sensor chip (GE Healthcare) to levels of ~6,000 response units (RU) using standard immobilization protocols (GE Healthcare). Experiments were carried out at 25 °C using HBS-P+ running buffer (GE Healthcare) containing 100 nM myristoyl-CoA. DDD85646 binding was tested by injecting varying concentrations of inhibitor (0.05 nM to 1,000 nM) at a flow rate of 30 µl min^{-1}. Different concentrations of DDD85646 were prepared so that the final DMSO concentration was 0.1%. Kinetic data analysis was performed using Biacore T100 Evaluation Software 2.0.1 and fitted to the standard 1:1 interaction model to give results.

Overexpression of NMT and mutant ARF1 studies. The plasmid vector pM2cN was a gift from D. Horn and S. Alsford. The *T. brucei NMT* open reading frame was amplified from genomic DNA using suitable primers and cloned into the plasmid vector pM2cN. The resulting construct encodes the target protein with an *N*-terminal Myc epitope tag under the control of a tetracycline-inducible T7 promoter. Mid-log phase *T. brucei* BSF 'single marker' (*T7RPOL TETR NEO*) s427 (subsequently termed SM) were electroporated with 10 µg of NotI-digested pM2cN-TbNMT using methods described[8]. Expression of Myc-tagged NMT was induced in stable cell lines by incubating parasites in 1 µg ml^{-1} tetracycline for 24 h. Immunoblotting[8] of parasite lysates was performed using the following primary antibodies: mouse anti-Myc (Invitrogen, 1:1,000 dilution), rabbit anti-TbNMT (1:500 dilution) and rabbit anti-BiP (gift from J. Bangs, used at 1:10,000 dilution), and mouse anti-α-tubulin, TAT1 (gift from K. Gull). Parental and NMT overexpressing cell lines (induced with tetracycline for 24 h) were seeded in 24-well plates at 5×10^5 ml^{-1} in triplicate, containing 0–100 nM of DDD85646. Motile cells were counted using a haemocytometer.

Production and transfection of the constructs pM2-TbARF1(Q71L) and pM2-TbARF1(G2A/Q71L) have been described previously[7]. Parental and mutant cell lines were seeded in 10 ml cultures at 5×10^5 ml^{-1}. DDD85646 (10 nM) with or without tetracycline (1 µg ml^{-1}) was added to cultures and flasks incubated at 37 °C with 5% CO_2 for 6 h. A set of cultures was set up in which tetracycline was added for 1 h before addition of DDD85646 and incubated for a further 5 h. Treated cells were then analysed using a Live/Dead two colour cell viability assay as described previously[7] and immunoblotted using anti-Myc antibody[8].

Transmission electron microscopy. *T. brucei* cells were collected by centrifugation at 1,000*g* for 10 min and fixed in 1 pellet-volume of 4% paraformaldehyde in 0.1 M piperazine-N,N′-bis(2-ethanesulphonic acid) for 30 min at room temperature (22–23 °C). Fixed cells were spun at 13,000*g* for 10 min, the supernatant was removed, and the pellet was resuspended in 1% aqueous osmium tetroxide (to fix and stain lipids), dehydrated, and set in Durcupan epoxy resin (Sigma). Sections were cut using a Leica Ultracut UCT system and analysed using a Philips Tecnai 12 transmission electron microscopy instrument.

Metabolic labelling. Live bloodstream form *T. brucei* (10^7) were incubated with and without 0.5 µM DDU85646 compound in 10 ml HMI9 for 6 h at 37 °C in a 5% CO_2 incubator and subsequently labelled with 50 µCi ml^{-1} [^{3}H]myristic acid or 20 µCi ml^{-1} [^{35}S]methionine for 1 h at 37 °C. The cells were washed in trypanosome dilution buffer and lysed in 1% Triton X-100 in 10 mM sodium phosphate buffer, pH 8 and incubated for 10 min at 37 °C. Duplicate aliquots of lysates were run in 4–12% Nupage gels, stained with Coomassie blue and subsequently treated, or not, with 0.2 M NaOH in MeOH for 1 h at room temperature (22–23 °C). The gels were washed and soaked in En^{3}Hance, dried and exposed to film.

Crystallography. LmNMT protein was obtained from the Structural Genomics Consortium parasitic disease project (courtesy of R. Hui). The protein construct consisted of 6xHis, TEV cleavage site and LmNMT 5–421, which was prepared in 10 mM HEPES, pH 7.5, 500 mM NaCl at 9 mg ml^{-1} for crystallization. A 200 mM stock solution of DDD85646 was prepared in DMSO and added to the protein solution to a final concentration of 10 mM. Myristoyl-CoA was also added to the sample to a final concentration of 1 mM before crystallization. Crystallization was carried out using vapour diffusion methods with 2 µl of protein–ligand complex mixed with 2 µl of reservoir solution. The reservoir solution contained 26% PEG 1500, 0.2 M NaCl, 0.1 M Na-cacodylate, pH 5.6. X-ray diffraction data for LmNMT + DDD85646 were measured at the European Synchrotron Facility at beamline ID14-1. The data were integrated and scaled using the HKL suite[35]. The structure was solved by molecular replacement as implemented in MOLREP[36] using the native LmNMT coordinates (PDB accession 3H5Z) as a search model. The structure was refined using REFMAC5[37] and manual alteration of the model carried out using COOT[38]. Ligand coordinates and topology files were created using the PRODRG server[39]. Data collection and refinement statistics are presented in Supplementary Table 1.

31. Thuita, J. K. *et al.* Efficacy of the diamidine DB75 and its prodrug DB289, against murine models of human African trypanosomiasis. *Acta Trop.* **108**, 6–10 (2008).
32. Sienkiewicz, N., Jaroslawski, S., Wyllie, S. & Fairlamb, A. H. Chemical and genetic validation of dihydrofolate reductase-thymidylate synthase as a drug target in African trypanosomes. *Mol. Microbiol.* **69**, 520–533 (2008).
33. Bowyer, P. W. *et al.* Molecules incorporating a benzothiazole core scaffold inhibit the N-myristoyltransferase of *Plasmodium falciparum*. *Biochem. J.* **408**, 173–180 (2007).

34. Räz, B., Iten, M., Grether-Bühler, M., Kaminsky, R. & Brun, R. The Alamar Blue® assay to determine drug sensitivity of African trypanosomes (*T.b.rhodesiense* and *T.b.gambiense*) *in vitro*. *Acta Trop.* **68,** 139–147 (1997).
35. Otwinowski, Z. & Minor, W. Processing of X-ray diffraction data collected in oscillation mode. *Methods Enzymol.* **276,** 307–326 (1997).
36. Vagin, A. & Teplyakov, A. MOLREP: an automated program for molecular replacement. *J. Appl. Cryst.* **30,** 1022–1025 (1997).
37. Murshudov, G. N., Vagin, A. A. & Dodson, E. J. Refinement of macromolecular structures by the maximum-likelihood method. *Acta Crystallogr. D* **53,** 240–255 (1997).
38. Emsley, P. & Cowtan, K. *Coot*: model-building tools for molecular graphics. *Acta Crystallogr. D* **60,** 2126–2132 (2004).
39. Schüttelkopf, A. W. & van Aalten, D. M. F. PRODRG: a tool for high-throughput crystallography of protein-ligand complexes. *Acta Crystallogr. D* **60,** 1355–1363 (2004).